Available online at www.sciencedirect.com
SCIENCE DIRECT®
Acta Materialia 52 (2004) 5083–5091
Acta MATERIALIA
www.actamat-journals.com

Magnetic field-induced reversible variant rearrangement in Fe–Pd single crystals

Tokujiro Yamamoto [a], Minoru Taya [a,*], Yuji Sutou [b], Yuanchang Liang [a], Taishi Wada [a], Larry Sorensen [c]

[a] *Center for Intelligent Materials and Systems, Department of Mechanical Engineering, University of Washington, Box 352600, Seattle, WA 98195-2600, USA*
[b] *Department of Materials Science and Engineering, Tohoku University, Aoba-ku, Sendai, Japan*
[c] *Department of Physics, University of Washington, Seattle, WA, USA*

Received 23 March 2004; received in revised form 8 July 2004; accepted 9 July 2004
Available online 19 August 2004

Abstract

Variant rearrangements induced by external magnetic field in Fe–Pd FCT martensite transformed from FCC austenite single crystals have been investigated by means of optical microscopy. Fe–Pd single crystals in fully martensite state contain two large correspondence variants, and a kink due to {1 0 1} twinning is observed at the twinning boundary of the variants. The twinning boundary exhibits both large reversible and small irreversible movement by applying magnetic field as a result of variant rearrangement, and 0.49% of reversible strain is obtained. The variant rearrangement is not completed even though magnetic flux density is increased to maximum of an electromagnet used. The boundary also moves reversibly by application of external compression stress, however, the direction of the boundary movement is opposite with respect to the movement induced by magnetic field and the variant rearrangment is not completed. The reversible strain of 2.8% was also observed when the specimen was compressed.

Keywords: Fe–Pd; Ferromagnetic shape memory alloy; Martensitic transformation

1. Introduction

Ferromagnetic shape memory alloys (FSMAs) have attracted a strong interest among actuator designers as possible fast responsive actuator materials. Earlier works on FSMAs were focused on phase transformation of Fe–Pd system [1] and Ni–Mn–Ga system [2] under temperature change. There are three mechanisms of actuation associated with FSMAs, under magnetic field which can be used as driving force for fast responsive actuator materials [3–7]: (i) magnetic field-induced phase transformation, (ii) martensite variant rearrangement and (iii) hybrid mechanism.

The first mechanism is based on the phase change from austenite to martensite under increasing magnetic field, or reverse phase transformation under decreasing magnetic field. If we can construct three dimensional phase transformation diagram of stress (σ)–temperature (T)–magnetic field (H) axes, see Fig. 1, the phase transformation of austenite to martensite phases under modest magnetic field, requires that the T–H phase boundary surface be inclined toward the T-axis with the T–H boundary line that has a smaller angle with T-axis, otherwise, the increasing H loading would not intersect the T–H phase boundary surface. Kato et al. [8] made preliminary estimate of the necessary magnetic energy to induce a phase transformation based on thermodynamic model, to conclude that large H field is required for the phase change to take for both Ni–

* Corresponding author. Tel.: +1 206 685 2850.
E-mail address: tayam@u.washington.edu (M. Taya).

1359-6454/$30.00
doi:10.1016/j.actamat.2004.07.014

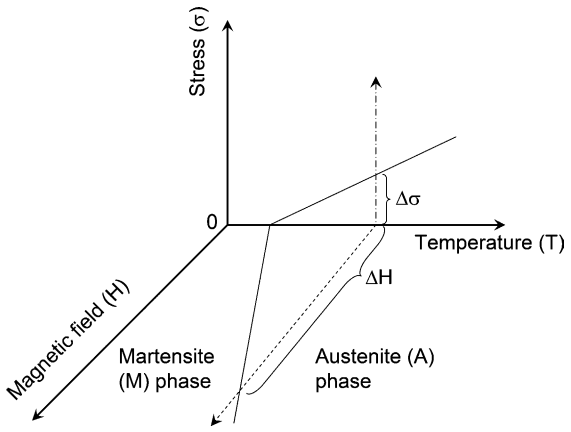

Fig. 1. 3-D phase transformation diagram of a FSMA under σ–T–H loading. It is noted that the magnitude of ΔH required of A → M phase change is large while $\Delta\sigma$ required for A → M phase change is small for most of FSMAs [8].

Mn–Ga and Fe–Pd. Therefore, this mechanism is not suited for use in designing compact actuators which may need a small and portable electromagnet system as a driving unit.

The second mechanism is to induce the strain in a FSMA with 100% martensite phase subjected to constant H-field which acts on the magnetic moments in magnetic domains that exist in the martensite phase so as to rotate them along the easy axis, i.e., c-axis in the case of Ni–Mn–Ga and Fe–Pd. The strain induced by this mechanism is a function of c/a ratio of FSMA, i.e., the order of shear strain, given by $a/c - c/a$. Thus, smaller the c/a ratio, the larger shear strain can be induced by this mechanism. The c/a ratio of Ni–Mn–Ga, is reported to be 0.94, which could provide 6% or more strain. Even though the strain induced by the second mechanism is very large, the corresponding stress remains to be modest as several MPa under modest applied magnetic flux density (1 T).

The third mechanism which we call as "hybrid mechanism", is based on a set of chain reactions, first applied magnetic flux (or field) gradient, magnetic force, stress induced martensite phase transformation (see Fig. 1), resulting in the phase change from stiff austenite to soft martensite phase, leading to large displacement. The advantages of this are large stress (hundred MPa in the case of Fe–Pd), modest – intermediate strain, fast actuation time. This phase change can be applied by approaching a compact and portable magnet close to the FSMA specimen which provides a large magnetic field gradient, thus, suited for use in designing actuators with large force capability.

The variant rearrangement mechanism (the second mechanism) is still useful for micro-electromechanical systems(MEMS)-based actuators as the order of force and stroke in a typical MEMS-based actuator is modest but, the fast speed of actuation is attractive to MEMS designers. Variant rearrangement in martensite has been also reported in Ni–Mn–Ga [10–14], Fe–Pt [15,16] and Ni–Mn–Al [17] systems. Some researchers proposed theoretical models for Ni–Mn–Ga system [2,9,18–22]. The order of reversible strain induced by magnetic field was only 0.2% in Ni_2MnGa in earlier study [10], it increased to 6% in a Ni_2MnGa single crystal with off-stoichiometric composition [23,24]. This remarkable improvement in the magnetic field-induced strain was achieved with external bias stress which helps converted variants to return to initial ones upon removal of magnetic field.

Fe–30at.%Pd ferromagnetic shape memory materials was first studied by Sohmura et al. [1]. This alloy exhib-

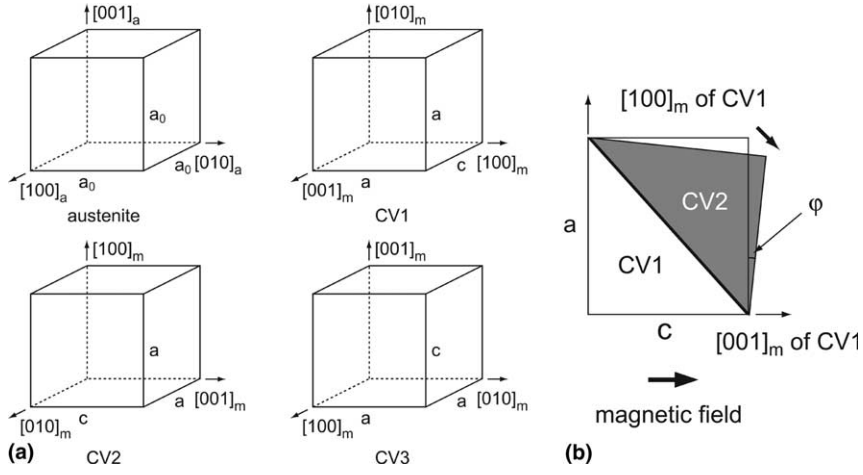

Fig. 2. (a) Unit cells of Fe–Pd FCC austenite and FCT martensite correspondence variants (CV1, CV2, CV3), where $[i\,j\,k]_a$ and $[i\,j\,k]_m$ are the coordinates based on austenite and martensite phase, respectively. (b) Unit cells of an initial variant (CV1) and a converted correspondence variant (CV2) by magnetic field applied along $[1\,0\,0]_a$ axis.

its martensitic transformation from face-centered cubic (FCC) to face-centered tetragonal (FCT) in this binary alloy system. James and Wuttig [2] reported that Fe–Pd alloy exhibited 0.6% of strain induced by applied constant magnetic field. When Fe–Pd FCC austenite transforms to FCT martensite, three types of martensite correspondence variants (CVs) take place since one of three *a*-axis of FCC austenite is selected as *c*-axis of FCT martensite (Fig. 2(a)) where unit cells of austenite and three martensite variants are shown [25]. The magnetic easy axis of an Fe–Pd martensite was identified to be *a*-axis [15]. When constant magnetic field is applied to Fe–Pd single crystal, variants are converted to other variants whose easy axes are parallel to the magnetic field direction in order to decrease magnetocrystalline energy. The change of a Fe–Pd FCT unit cell by constant magnetic field along *c*-axis of an initial variant is illustrated in Fig. 2(b). An initial variant (CV1) whose easy axis (*a*-axis) is perpendicular to the applied magnetic field is converted to another variant (CV2) whose easy axis is almost parallel to the magnetic field with introducing twinning, whose plane of shear is $\{1\ 0\ 1\}$ and and direction of shear is $\langle 1\ 0\ \bar{1}\rangle$. The strain and the angle between *a*-axis of CV1 and *c*-axis of CV2, denoted as φ in Fig. 2(b), are produced by conversion of CV1 to CV2, and they can be geometrically expressed by means of tetragonality, *c*/*a* ratio, Table 1, where the relation among *c*/*a* ratio, expected strain and angle φ are calculated based on the formulation in Appendix A. By choosing optimum alloy composition, one could obtain more than 5% of strain by the variant rearrangement mechanism. Variant rearrangement is not clearly observed in a polycrystalline Fe–Pd specimens due to constraints of adjacent grains. The order of reversible strain reported by others remains modest, 0.6% [2]. In the present paper, we shall report reversible magnetic field-induced strain in Fe–Pd single crystals and discuss its mechanism.

Table 1
Expected strain and angle φ caused by variant rearrangements

c/*a* Ratio	Strain (%)	Angle φ (°)
0.98	2.02000	1.15745
0.96	4.07993	2.33828
0.94	6.17966	3.54294
0.92	8.31889	4.77189
0.90	10.49724	6.02558

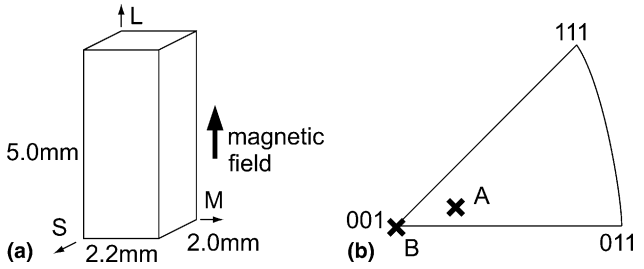

Fig. 3. (a) Dimension and direction of specimens A and B, and (b) crystallographic orientation of applied magnetic field.

2. Experimental procedure

A number of small master ingots of Fe–30.5at.%Pd were prepared by Ar arc-melting high-purity Fe chunks and Pd powders. Lattice parameters of Fe–30.5at.%Pd were measured by X-ray diffractometry (XRD) at −100 °C. The master ingots were set in the Bridgeman furnace at DOE AMES Laboratory. Then single crystal specimens were grown by the Bridgeman method. The single crystals of Fe–Pd austenite were heat-treated at 1300 °C for 72 h in Ar atmosphere and then quenched into water to obtain FCC austenite phase. Back Laue reflection method was used to determine the crystallographic orientation of the specimens. Three specimens in austenite state were cut into parallelepiped rectangular (2.0 mm × 2.2 mm × 5.0 mm) by a diamond wheel saw and polished. One of them was used to measure martensitic transformation temperature. Directions along longer, middle and shorter edges are denoted as *L*, *M* and *S*, respectively (Fig. 3(a)). Miller indices of the orientation of *L*, *M* and *S* directions are listed in Table 2 for specimens A and B. For sample B, all edges were cut perpendicular to $\langle 100\rangle_a$ and all surfaces were parallel to $\{1\ 0\ 0\}_a$. Martensitic transformation temperatures were measured by differential scanning calorimetry (Perkin–Elmer, DSC 6). Observation setup is illustrated in Fig. 4 schematically. A specimen clamped to fix was dipped into ethanol to prevent the specimen surfaces from being fogged and to keep specimen temperature uniform during observation. Then the specimen was indirectly cooled by use of pieces of dry ice to temperature lower than martensite finish temperature (M_f) without magnetic field. The temperature of the specimen was monitored by a thermo-couple set near the specimen. The specimen surfaces were observed by means of a CCD camera. Constant magnetic field was applied along

Table 2
Indices of crystallographic orientations of specimen A and B

	S	*M*	*L*
A	[0.276 0.643 −0.719]	[0.105 −0.766 −0.629]	[0.956 −0.105 0.276]
B	[1 0 0]	[0 1 0]	[0 0 1]

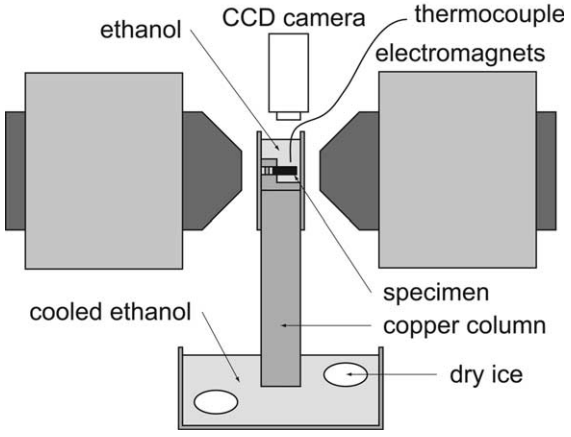

Fig. 4. Schematic illustration of observation setup of a specimen with and without magnetic field.

the longer side of the specimens by an electromagnet (GMW Magnet Systems, Model 5403 Electromagnet).

3. Results

3.1. martensite transformation temperature and crystallography of specimens

Martensitic transformation temperatures of a Fe–Pd single crystal specimen were determined by differential scanning calorimetry (DSC) measurements and the results are shown in Fig. 5 from which martensite start (M_s), M_f, reverse transformation start (A_s) and reverse transformation finish (A_f) temperature are determined as, $M_s = 6$ °C, $M_f = 0$ °C, $A_s = 10$ °C, $A_f = 16$ °C. The composition of the specimen is almost homogenous, because only one peak is detected in the DSC measurements and baseline of the DSC profile is flat. We found that the lattice parameter of FCC austenite is $a_0 = 0.375016$ nm and those of FCT martensite are

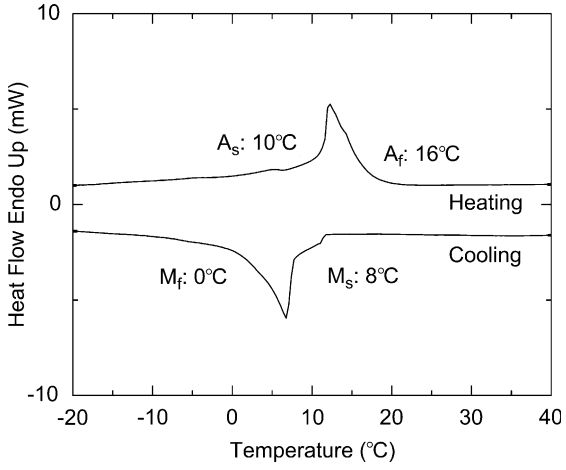

Fig. 5. DSC curves of a single crystal specimen.

$a = 0.379001$ nm and $c = 0.369526$ nm from XRD results. Constant magnetic field was applied along the L-direction of two different specimens with different crystallographic orientations in order to clarify dependence on the direction of applied magnetic field. The angle between the direction of the applied magnetic field and $[0\ 0\ 1]_a$ is 16° and 0° for specimens, A and B, respectively. Reversible variant rearrangements were observed in these two specimens. It should be noted here that we focused on one twinning boundary which makes an large kink and clear bright and dark contrast although a few minor variants were also observed on the surface of both specimens A and B while the specimens were cooled lower temperature than M_f.

3.2. Specimen A

Fig. 6 shows one of the surfaces of specimen A observed at around −20 °C without magnetic field. As noted before, the composition of this specimen is homogeneous and the whole specimen was in martensite state, according to the result of DSC measurements. One straight trace is clearly observed in Fig. 6 and it corresponds to (1 0 1) plane of martensite. The trace is caused by (1 0 1) twinning plane between two large CVs. Because of a kink by twinning, the bright and dark contrast is generated. Fig. 7 shows such twinning plane boundaries observed be-

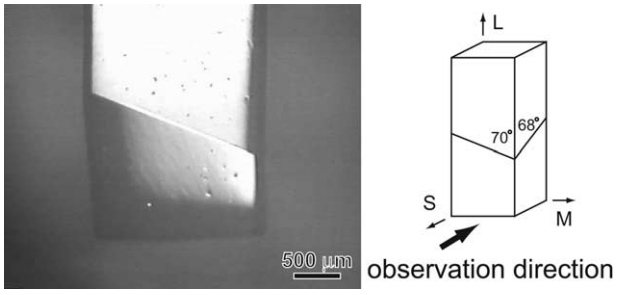

Fig. 6. Trace of a twinning plane observed in specimen A as cooled to −20 °C.

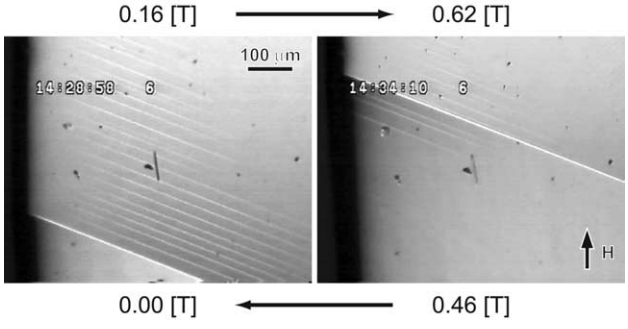

Fig. 7. Reversible movement of the twinning plane trace observed in specimen A by magnetic field applied along the indicated arrow with H.

fore and after its boundary moving by application of magnetic field. The twin boundary started to move upward when magnetic flux density reached 0.16 T and continued to move with increasing magnetic flux density until it reached 0.62 T. Then its movement stopped beyond magnetic flux density of 0.62 T. The distance of the twin boundary movement was about 320 μm and its speed was 2 mm s^{-1}. The plane also started to move back to the initial position at 0.46 T and finished moving at 0.00 T. Faint line-shaped bright or dark areas observed in Fig. 7 are probably another CVs introduced as planer defects, which were left in a major CV during the movement of the boundary. The morphology of CVs in the specimen is similar to that observed in Ni–Mn–Ga [18,24] rather than that observed in Fe–Pd by James and Wuttig [2] and Fukuda and Kakeshita [26] The morphology reported by James et al. likely consists of several habit plane variants, and Fukuda et al. reported stripes of narrow variant plates during increasing magnetic flux density.

3.3. Specimen B

Fig. 8 shows the surface morphology observed in specimen B by applying magnetic field where horizontal arrow markers are stationary reference locations. The surface morphology observed in this specimen is similar to that observed in specimen A. The twin boundary started moving when the magnetic flux density reached 0.12 T and it stopped at 0.39 T, even though the magnetic flux density was increased to maximum of the electromagnet used, i.e., 1.2 T. In decreasing the magnetic flux density, the twin boundary went back to the initial position that was observed under the magnetic flux density between 0.27 and 0.00 T. As the twin boundary moved 490 μm upward and downward by increasing and decreasing of the magnetic flux density, 9.7% of volume fraction in specimen B participated in the variant rearrangement by applying magnetic field. The specimen B exhibited 25 μm displacement along *L*-direction of the specimen by application of magnetic field, resulting in 0.49% of strain. To clarify the effect of the stress generated by the clamping used in the present study, specimen B without the clamp was heated up to 40 °C, and the specimen was cooled to −20 °C, then the same surface of the specimen was observed. Fig. 9 shows the position of the twining plane boundary observed on the surface of specimen B (a) before applying magnetic field, (b) with magnetic flux density of 0.5 T and (c) after removing magnetic field (0.0 T). As shown in Fig. 9, the movement of the boundary was not completely reversible. The position of the boundary after removing magnetic field was different from that before applying magnetic field and small amount of irreversible displacement was observed. This irreversible displacement was small even though specimen B was applied magnetic field without clamping. This indicates that clamping causes bias stress inside of specimens, however, its effect on the displacement is considered small.

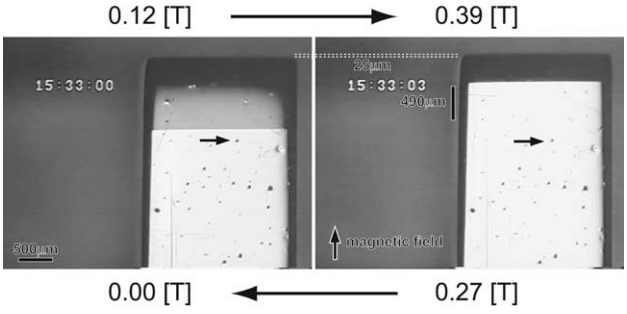

Fig. 8. Movement of a twinning plane and elongation observed in specimen B along $[1\ 0\ 0]_a$ by applying magnetic field. The black arrows indicate a mark for identifying the same fixed reference point.

Compression stress was manually applied to specimen B by using a caliper along *L* direction. With increasing stress, the twinning boundary similar to those of Figs. 8 and 9 moved downward with increasing the dark contrast area (Fig. 10(a)–(d)). When the stress was removed, the boundary went back to the initial position. The initial length of specimen B was 4.97 mm. The minimum length of the specimen was about 4.83 mm under the maximum compression stress, and the amount of the reversible stress-induced strain was estimated as 2.8%. Because *c*/*a* ratio of a martensite variant is smaller than one, the variants in the specimen converted to the preferred variants whose *c*-axis is parallel to the loading axis. The twin-

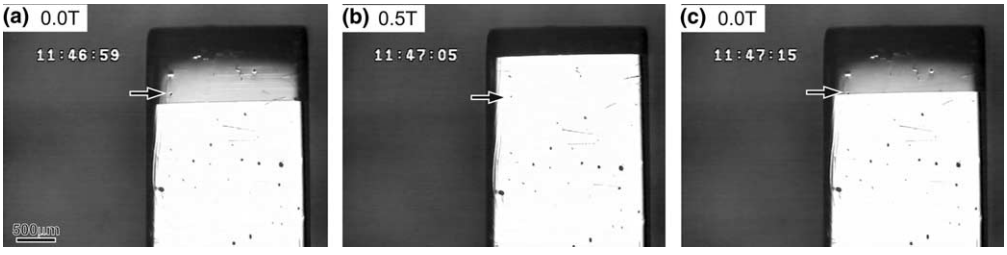

Fig. 9. Reversible and Small amount of irreversible movement of a twinning plane observed in specimen B. The arrows indicate a reference mark for identifying the same location. (a) Before first application of magnetic field (0.0 T), (b) under first application of magnetic field (0.5 T) and (c) after first application of magnetic field (0.0 T).

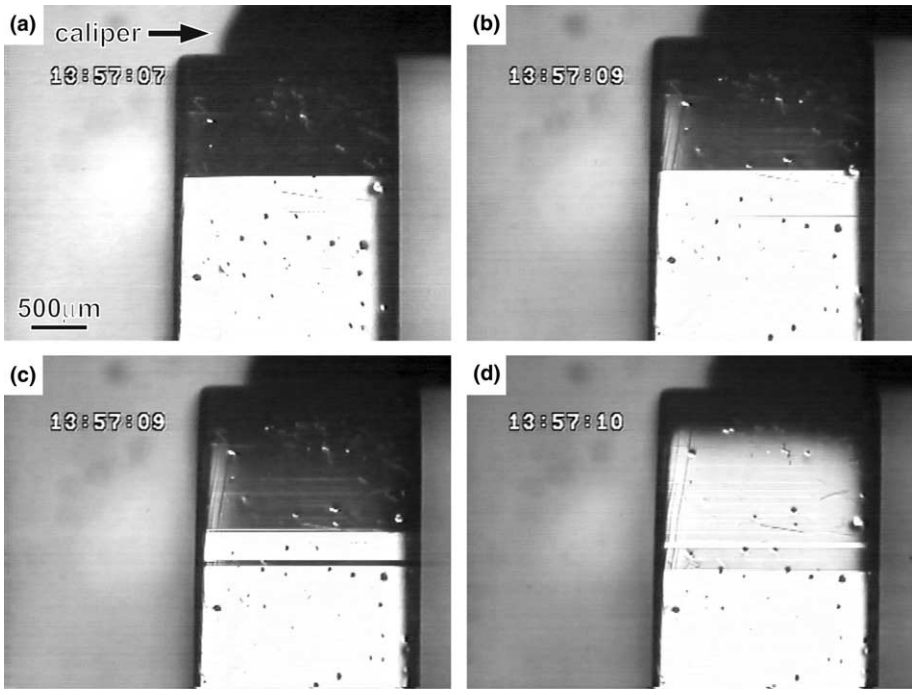

Fig. 10. Stress-induced variant rearrangement observed at −20 °C. Pictures from (a) to (d) were taken during increasing compression stress.

ning boundary movement by applying magnetic field or compression stress implies that the magnetic easy axes are *a*-axes in Fe–Pd FCT martensite, as reported by Cui and James [27].

Stress-induced reversible variant rearrangement which was observed in some shape memory alloys, known as rubber-like behavior or twinning pseudoelasticity, requires long time aging at low temperature to induce microstructural change [28,29]. The specimens used in this study are not subjected to aging at such temerature. However, they exhbited reversible variant rearrangement induced by both external stress and external magnetic field.

4. Discussion

4.1. Magnetic field-induced strain

If we use an infinitesimal deformation approach and the coordinate system is taken as the austenite system, transformation strains caused by martensitic transformation from FCC austenite unit cell to FCT martensite CVs in Fe–Pd are given by [25]

$$\varepsilon^{\mathrm{T}}(1)=\begin{bmatrix}\varepsilon_c & 0 & 0\\ 0 & \varepsilon_a & 0\\ 0 & 0 & \varepsilon_a\end{bmatrix}\quad \text{in CV1}, \tag{1}$$

$$\varepsilon^{\mathrm{T}}(2)=\begin{bmatrix}\varepsilon_a & 0 & 0\\ 0 & \varepsilon_c & 0\\ 0 & 0 & \varepsilon_a\end{bmatrix}\quad \text{in CV2}, \tag{2}$$

$$\varepsilon^{\mathrm{T}}(3)=\begin{bmatrix}\varepsilon_a & 0 & 0\\ 0 & \varepsilon_a & 0\\ 0 & 0 & \varepsilon_c\end{bmatrix}\text{in CV3}, \tag{3}$$

$$\varepsilon_a=\frac{a-a_0}{a_0}, \tag{4}$$

$$\varepsilon_c=\frac{c-a_0}{a_0}. \tag{5}$$

And the strain caused by variant rearrangement from CV1 to CV2 is derived from Eqs. (1) and (2).

$$\varepsilon=\begin{bmatrix}\varepsilon_a-\varepsilon_c & 0 & 0\\ 0 & -(\varepsilon_a-\varepsilon_c) & 0\\ 0 & 0 & 0\end{bmatrix}=\begin{bmatrix}0.0252656 & 0 & 0\\ 0 & -0.0252656 & 0\\ 0 & 0 & 0\end{bmatrix}. \tag{6}$$

Here, the lattice parameters of austenite and martensite of Fe–30.5at.%Pd measured at −100 °C by means of XRD are used. If the strain caused by variant rearrangement is geometrically and exactly calculated based on the geometry of Fig. 2(b) and Fig. 13 in Appendix A, we obtain

$$\varepsilon = \begin{bmatrix} \frac{1-(c/a)^2}{1+(c/a)^2} & 0 & 0 \\ 0 & -\frac{1-(c/a)^2}{1+(c/a)^2} & 0 \\ 0 & 0 & 0 \end{bmatrix} = \begin{bmatrix} 0.0253123 & 0 & 0 \\ 0 & -0.0253123 & 0 \\ 0 & 0 & 0 \end{bmatrix}. \tag{7}$$

Since Eq. (6) is nearly equal to Eq. (7), the infinitesimal deformation approach is reasonable in estimate of change in transformation strain.

The *c*/*a* ratio depends on the composition of the specimen and the specimen temperature. According to the results reported by Oshima [30], *c*/*a* ratio of Fe–Pd FCT martensite decreases both with decreasing Pd content of the specimen and decreasing the specimen temperature. In the present study, we observed 0.49% of reversible magnetic field-induced strain due to variant rearrangement of 9.7% of volume percent of specimen B at −20 °C. If all the variants (CV1) in specimen B were converted to the others (CV2), the strain estimated would be 5.1%. This value is twice as large as the strain estimated for Fe–30.5at.%Pd by both the infinitesimal deformation approach and geometrical calculation Eqs. (6) and (7), and this is because the *c*/*a* ratio of the specimen B is smaller than the *c*/*a* ratio of Fe–30.5at.%Pd measured in this study, 0.975. Since the observation temperature of specimen B is higher than the XRD measurement temperature for Fe–30.5at.%Pd, the difference of the experimental results and the estimations is caused by the decreasing Pd content of the specimen from 30.5at.%Pd during the growth of the single crystals. From the observed strain and the volume ratio of converted CVs the *c*/*a* ratio of specimen B at −20 °C is estimated to be about 0.950.

4.2. Magnetization vector in variants

Specimen B consists of CV1 and CV2, as shown in Fig. 11, and $(0\,1\,0)_a$ face is kinking and bright and dark contrast is caused while $(0\,0\,1)_a$ face is flat. When the magnetic field is applied along $[1\,0\,0]_a$ direction, CV1 is converted to CV2 or CV3, however, the existing CV (CV2) will be selected in the conversion, because conversion from CV1 to CV3 increases free energy in the specimen by producing new twin boundary energy. The width of CV2 increases while keeping the same number of the twinning boundaries as the applied magnetic flux density increases. The above hypothesis agrees with the present experimental results.

Suppose that a specimen consists of one CV1 and one CV2 and that a twinning boundary, whose area is denoted as S, moves by Δx when magnetic field increases to H (Fig. 12). Here, we asume that magnetization vectors do not rotate during the boundary movement. Magnetic energy for CV1 and CV2, $E_{\mathrm{mag},1}$ and $E_{\mathrm{mag},2}$, before the boundary movement are approximately denoted as follows.

$$E_{\mathrm{mag},1} = \left\{ -MH\cos\theta + K_{\mathrm{u1}}\sin^2\left(\frac{\pi}{2} - \theta\right) \right\} \cdot V_1, \tag{8}$$

$$E_{\mathrm{mag},2} = -MH \cdot V_2, \tag{9}$$

where V_1 and V_2 are volume of CV1 and CV2, respectively, and M is intensity of magnetization of martensite, K_{u1} is uniaxial anisotropy constant of martensite, θ is the angle between the direction of the magnetic field and the magnetization of CV1, m_1. And magnetic energy

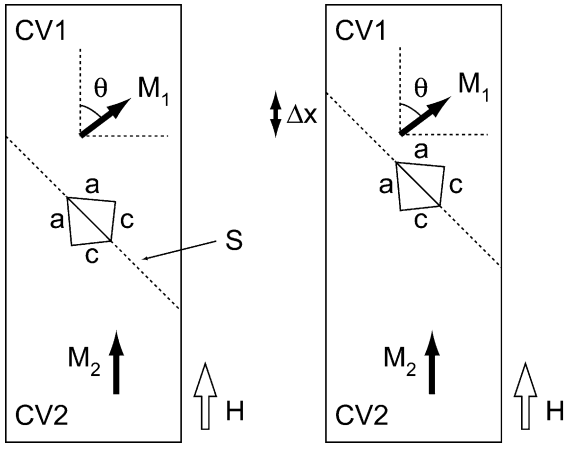

Fig. 12. Magnetization vector m_1 and m_2 in CV1 and CV2 during twinning boundary movement.

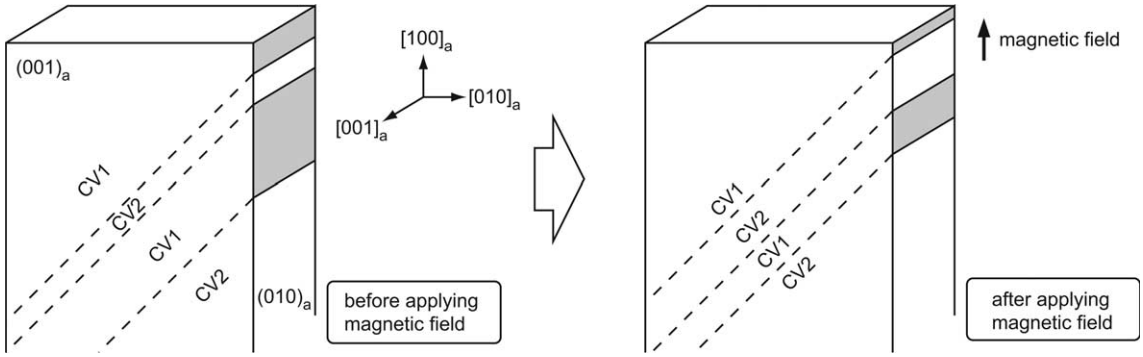

Fig. 11. Schematic illustration of variant rearrangements by magnetic field and surface morphology change.

for CV1 and CV2 after the movement, $E'_{\mathrm{mag},1}$ and $E'_{\mathrm{mag},2}$ are expressed as

$$E'_{\mathrm{mag},1} = \left\{-MH\cos\theta + K_{u1}\sin^2\left(\frac{\pi}{2}-\theta\right)\right\}\cdot(V_1 - S\Delta x), \tag{10}$$

$$E'_{\mathrm{mag},2} = -MH\cdot(V_2 + S\Delta x). \tag{11}$$

The change of magnetic energy during the boundary movement is derived as below.

$$\begin{aligned}\Delta E_{\mathrm{mag}} &= \left(E'_{\mathrm{mag},1} - E_{\mathrm{mag},1}\right) + \left(E'_{\mathrm{mag},2} - E_{\mathrm{mag},2}\right)\\ &= \left\{MH(1-\cos\theta) + K_{u1}\cos^2\theta\right\}\cdot S\Delta x.\end{aligned} \tag{12}$$

As this energy change is dissipated by work done by the boundary movement, ΔW_{fric},

$$\Delta W_{\mathrm{fric}} = -\tau\cdot S\Delta x, \tag{13}$$

$$\Delta E_{\mathrm{mag}} + \Delta W_{\mathrm{fric}} = 0, \tag{14}$$

where τ is friction stress of the boundary movement. If the boundary movement progresses by the expansion of a twinning dislocation loop, τ = 1.4 MPa [31]. From these equations, by substituting $H = 0.4$ T $= 3.18\times10^6$ A m^{-1}, $M = 1.571$ Wb m^{-2} [32], $K_{u1} = 3.1\times10^4$ J m^{-3} [27], we can estimate the angle θ as

$$\theta = 43.7^\circ. \tag{15}$$

Though we can estimate the angle between the magnetization of CV1 and the magnetic field, we cannot clarify the reason why the twinning boundary moves reversibly by application of neither magnetic field nor compression stress in this study.

5. Conclusion

The surface morphology and variant rearrangement in Fe–Pd single crystals have been investigated.

1. The specimens exhibit both reversible strain of about 0.5% without external bias stress and small amount of irreversible strain induced by applying magnetic field. The boundary of two CVs moves continueously by increasing and decreasing magnetic flux density so that the volume ratio of CV whose magnetic easy axis, *a*-axes, increases. Although the magnetic flux density increases up to 1.2 T, the variants whose *c*-axis is parallel to the direction of magnetic field do not convert to the other variants whose *a*-axis is parallel to the magnetic field direction.
2. The reversible CVs rearrangement is also observed by applying external compression stress. When the compression stress is applied, the volume ratio of CV whose *c*-axis is parallel to the loading axis increases. As a result, the boundary of the two CVs moves towards opposite direction with respect to the boundary movement observed in applying magnetic field. This reversible strain is observed without aging at such temperature that microstructural change may occur.

Acknowledgements

This work was supported by National Science Foundation (CMS-0303536) where Dr. Jorn Larsen-Basse and Dr. Yip-Wah Chung are the program monitor. The authors acknowledge helpful discussions with Dr. Setsuo Kajiwara, NIMS, Japan and Dr. Tsutomu Mori, UMIST, United Kingdom, and sample preparation of Fe–Pd single crystals by Dr. Thomas Lograsso, DOE Laboratory, AMES, Iowa.

Appendix A

Referred to Fig. 13, angles $\angle APB$ and $\angle AP'B$ are 90°, points A, B, P, P' are on the arc of the same circle whose center is O' and diameter is AB. If the radius of the circle and $\angle PO'B$ is defined as r and α,

$$r = O'A = O'B = \frac{1}{2}\sqrt{a^2+c^2},$$

$$\cos\theta = \frac{c}{2r},$$

$$\sin\theta = \frac{a}{2r},$$

$$PP' = 2r\cos\alpha,$$

$$\cos 2\theta = \cos^2\theta - \sin^2\theta = \frac{c^2}{a^2+c^2} - \frac{a^2}{a^2+c^2} = \frac{c^2-a^2}{c^2+a^2},$$

$$\cos\alpha = \cos(\pi - 2\theta) = -\cos 2\theta = \frac{a^2-c^2}{a^2+c^2}.$$

Here, we define $\overrightarrow{OP}$ and $\overrightarrow{OP'}$ as follows,

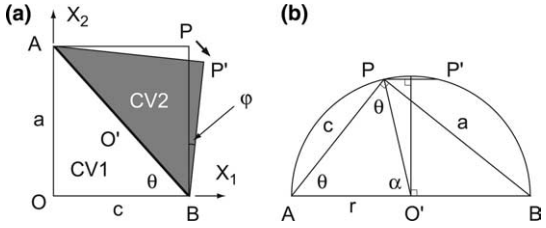

Fig. 13. (a) Geometry of variant CV1 converted to CV2. (b) Two variant rearrangement of CV1 → CV2.

$$\overrightarrow{OP} = \begin{bmatrix} x_1 \\ x_2 \\ x_3 \end{bmatrix},$$

$$\overrightarrow{OP'} = \begin{bmatrix} x'_1 \\ x'_2 \\ x'_3 \end{bmatrix},$$

and we obtain the following relationship

$$\cos\theta = \frac{OA}{AB} = \frac{x_1}{2r},$$

$$\sin\theta = \frac{OB}{AB} = \frac{x_2}{2r},$$

$x'_1,\ x'_2,\ x'_3$ are expressed by using $x_1,\ x_2,\ x_3$

$$x'_1 = x_1 + PP'\cos\theta = x_1 + 2r\cos\alpha\cos\theta = x_1 + x_1\cos\alpha,$$

$$x'_2 = x_2 - PP'\sin\theta = x_2 - 2r\cos\alpha\sin\theta = x_2 - x_2\cos\alpha,$$

$$x'_3 = x_3.$$

Therefore, the strain ε caused by variant rearrangement is derived as follows:

$$\begin{bmatrix} x'_1 \\ x'_2 \\ x'_3 \end{bmatrix} = \begin{bmatrix} 1+\cos\alpha & 0 & 0 \\ 0 & 1-\cos\alpha & 0 \\ 0 & 0 & 1 \end{bmatrix} \begin{bmatrix} x_1 \\ x_2 \\ x_3 \end{bmatrix},$$

$$\varepsilon = \begin{bmatrix} \cos\alpha & 0 & 0 \\ 0 & -\cos\alpha & 0 \\ 0 & 0 & 0 \end{bmatrix} = \begin{bmatrix} \frac{1-(c/a)^2}{1+(c/a)^2} & 0 & 0 \\ 0 & -\frac{1-(c/a)^2}{1+(c/a)^2} & 0 \\ 0 & 0 & 0 \end{bmatrix}.$$

Shear s is also expressed as follows:

$$s = 2\frac{PP'}{r\sin\alpha} = \frac{a^2-c^2}{ac} = (a/c)\{1-(c/a)^2\}.$$

We have the following relationship:

$$\varphi = \theta - \left(\frac{\pi}{2} - \theta\right) = 2\theta - \frac{\pi}{2} = \frac{\pi}{2} - \alpha,$$

$$\sin\varphi = \cos\alpha = \frac{a^2-c^2}{a^2+c^2}.$$

Therefore, angle φ is derived as

$$\varphi = \sin^{-1}\cos\alpha = \sin^{-1}\left(\frac{1-(c/a)^2}{1+(c/a)^2}\right).$$

References

[1] Sohmura T, Oshima R, Fujita FE. Scr Metall 1980;14:855–6.
[2] James RD, Wuttig M. Philos Mag A 1998;77:1273–99.
[3] Liang Y, Kato H, Taya H. In: Proceedings of the Plasticity '00: 8th International Symposium on Plasticity and Current Applications, 193, 2000.
[4] Liang Y, Kato H, Taya M, Mori T. Scr Mater 2001;45:569.
[5] Murray SJ, Frinelli M, Kantner C, Huang JK, Allen SM, O'Handley RC. J Appl Phys 1998;83:7297.
[6] James RD, Tickle R, Wuttig M. Mater Sci Eng A 1999;273:320.
[7] Ullakko K, Huang JK, Kokorin VV, O'Handley RC. Scr Mater 1997;36:1133.
[8] Kato H, Wada T, Tagawa T, Liang Y, Taya M. In: Proceedings of 50th Anniversary of Japan Society of Material Sciences, Osaka, May 21–26, 296, 2001.
[9] Wada T, Taya M. Proc SPIE, Smart Struct Mater 2002;294: 4699.
[10] Ullakko K, Huang JK, Kantner C, O'Handley RC, Kokorin VV. Appl Phys Lett 1996;69:1966–8.
[11] Sozinov A, Ezer Y, Kimmel G, Yakovenko P, Giller D, Wolfus Y, et al. J Phys IV 2001;11:Pr8-311–16.
[12] Sozinov A, Likhachev AA, Ullakko K. Proc SPIE 2001;4333:189–96.
[13] Sozinov A, Likhachev AA, Ullakko K. Proc SPIE 2001;4333:197–206.
[14] O'Handley RC, Allen SM, Paul DI, Henry CP, Marioni M, Bono D, et al. Proc SPIE 2003;5053:200–6.
[15] Sakamoto T, Fukuda T, Kakeshita T, Takeuchi T, Kishio K. J Appl Phys 2003;93:8647–9.
[16] Kakeshita T, Takeuchi T, Fukuda T, Tsujiguchi M, Saburi T, Oshima R, et al. Appl Phys Lett 2000;77:1502–4.
[17] Fujita A, Fukamichi K, Gejima F, Kainuma R, Ishida K. Appl Phys Lett 2000;77:3054–506.
[18] Likhachev AA, Ullakko K. Phys Lett A 2000;275:142–51.
[19] Likhachev AA, Ullakko K. Eur Phys J B 2000;14:263–7.
[20] Likhachev A, Ullakko K. J Magn Magn Mater 2001;226–230:1541–3.
[21] O'Handley RC. J Appl Phys 1998;83:3263–70.
[22] O'Handley RC, Allen SM, Paul DI, Henry CP, Marioni M, Bono D, et al. Proc SPIE 2003;5053:200–6.
[23] Murray SJ, Marioni M, Allen SM, O'Handley RC, Lograsso TA. Appl Phys Lett 2000;77:886–8.
[24] Murray SJ, O'Handley RC, Allen SM. J Appl Phys 2001;89:1295–301.
[25] Kato H, Wada T, Liang Y, Tagawa T, Taya M, Mori T. Mater Sci Eng A 2002;332:134–9.
[26] Fukuda T, Kakeshita T. Netsushori 2003;43:137–42 [in Japanese].
[27] Cui J, James RD. IEEE Trans Magnet 2001;37:2675–7.
[28] Tsuchiya T, Tateyama K, Sugino K, Marukawa K. Scr Metall Mater 1995;32:259–64.
[29] Otsuka K, Ren Xiaobing. Mater Sci Eng A 2001;312:207–18.
[30] Oshima R. Scr Metall 1981;15:829–33.
[31] Liang Y, Wada T, Kato H, Tagawa T, Taya M, Mori T. Mater Sci Eng A 2002;338:89–96.
[32] Wada T, Liang Y, Kato H, Tagawa T, Taya M, Mori T. Mater Sci Eng A 2003;361:75–82.